Ocean Dynamics (2014) 64:507–517
DOI 10.1007/s10236-014-0702-0

High-frequency internal wave motions at the ANTARES site in the deep Western Mediterranean

Hans van Haren · The ANTARES Collaboration

Received: 29 May 2013 / Accepted: 28 January 2014 / Published online: 22 February 2014

Abstract High-frequency internal wave motions of periods down to 20 min have been observed in a yearlong record from the deep Western Mediterranean, mainly in vertical currents. The observations were made using the ANTARES neutrino telescope infrastructure. One line of the telescope is instrumented with environmental monitoring devices, and in particular with an Acoustic Doppler Current Profiler that was used to measure currents around 2,200 m. Such high-frequency internal waves are commonly observed much closer to the sea surface where the vertical density stratification is more stable than in the deep sea. In this paper, they are supported by the relatively large stratification following newly formed dense water. During the severe winters of 2005 and 2006, deep dense-water formation occurred in the Ligurian subbasin. Its collapse and spread over the sea floor across the basin remained detectable for at least 3 years as deduced from the present yearlong current record, which is from 2008. The observed high-frequency internal waves match the occasional density stratification observed in ~1-m-thin layers using previous shipborne conductivity–temperature–depth measurements. Such layers and waves are relatively unusual in the deep Mediterranean, where commonly several hundreds-of-meters-thick near-homogeneous layers dominate. Such thick near-homogeneous layers provide about a half-decade narrow internal wave band around the inertial frequency (f). In contrast, the presently observed vertical currents occasionally show a "small-scale" internal wave band that is on average 1.5 decades wide, associated with thin-layer stratification. In spite of its relatively large width, this band still shows variance peaking near f rather than near the large-scale buoyancy frequency N (= 2.3–4.5f) and this variance is found to increase with increasing N.

Keywords High-frequency internal waves · Deep Western Mediterranean · Vertical current spectra with inertial peak · Positive power law in stratification

Responsible Editor: Pierre De Mey

The ANTARES Collaboration is composed of the following: S. Adrián-Martínez, I. Al Samarai, A. Albert, M. André, M. Anghinolfi, G. Anton, L. Anton, S. Anvar, M. Ardid, T. Astraatmadja, J-J. Aubert, B. Baret, S. Basa, V. Bertin, S. Biagi, C. Bigongiari, C. Bogazzi, B. Bouhou, M.C. Bouwhuis, J. Brunner, J. Busto, A. Capone, C. Cârloganu, J. Carr, S. Cecchini, Z. Charif, Ph. Charvis, T. Chiarusi, M. Circella, F. Classen, R. Coniglione, L. Core, H. Costantini, P. Coyle, A. Creusot, C. Curtil, G. De Bonis, M.P. Decowski, I. Dekeyser, A. Deschamps, C. Distefano, C. Donzaud, D. Dornic, Q. Dorosti, D. Drouhin, T. Eberl, U. Emanuele, A. Enzenhöfer, J-P. Ernenwein, S. Escoffier, K. Fehn, P. Fermani, M. Ferri, S. Ferry, V. Flaminio, F. Folger, U. Fritsch, J-L. Fuda, S. Galatà, P. Gay, S. Geißelsöder, K. Geyer, G. Giacomelli, V. Giordano, A. Gleixner, J.P. Gómez-González, K. Graf, G. Guillard, G. Hallewell, M. Hamal, A.J. Heijboer, Y. Hello, J.J. Hernández-Rey, B. Herold, J. Hößl, C.C. Hsu, C. James, M. de Jong, M. Kadler, O. Kalekin, A. Kappes, U. Katz, P. Kooijman, C. Kopper, A. Kouchner, I. Kreykenbohm, V. Kulikovskiy, R. Lahmann, G. Lambard, G. Larosa, D. Lattuada, D. Lefevre, E. Leonora, D. Lo Prest, H. Loehner, S. Loucatos, F. Louis, S. Mangano, M. Marcelin, A. Margiotta, J.A. Martínez-Mora, S. Martini, A. Meli, T. Montaruli, M. Morganti, H. Motz, C. Mueller, M. Neff, E. Nezri, D. Palioselitis, G.E. Păvălaş, J. Petrovic, P. Piattelli, V. Popa, T. Pradier, C. Racca, C. Reed, G. Riccobene, R. Richter, C. Rivière, A. Robert, K. Roensch, A. Rostovtsev, J. Ruiz-Rivas, M. Rujoiu, D. F. E. Samtleben, A. Sánchez-Losa, P. Sapienza, J. Schmid, J. Schnabel, S. Schulte, F. Schüssler, T. Seitz, R. Shanidze, F. Simeone, A. Spies, M. Spurio, J.J.M. Steijger, Th. Stolarczyk, M. Taiuti, C. Tamburini, A. Trovato, B. Vallage, C. Vallée, V. Van Elewyck, P. Vernin, E. Visser, S. Wagner, G. Wijnker, J. Wilms, E. de Wolf, K. Yatkin, H. Yepes, D. Zaborov, J.D. Zornoza, J. Zúñiga.

H. van Haren (✉)
Royal Netherlands Institute for Sea Research (NIOZ), P.O. Box 59, Den Burg 1790 AB, the Netherlands
e-mail: hans.van.haren@nioz.nl

1 Introduction

Although internal gravity waves are omnipresent in seas and oceans, and they are thought to dominate vertical turbulent mixing when they break above underwater topography, they

are not expected to largely influence waters in the deep Mediterranean Sea. This is because in general the vertical density stratification is very low there, with homogeneous layers of hundreds of meters thick (e.g., van Haren and Millot 2004; Schroeder et al. 2008). When the density stratification, i.e., the main force generating high-frequency internal waves, becomes negligible, a narrow internal wave frequency (σ) band is expected with small variance.

Recent developments and investigations suggest that, in contrast to the above image, the deep Mediterranean can support considerable internal wave motions. First, near-homogeneous deep Mediterranean waters have demonstrated the presence of propagating internal waves and vertical motions having O(0.01 m s^{-1}) amplitudes, near the local inertial frequency (f) (van Haren and Millot 2004, 2005). Normally, f is understood as the lowest internal wave frequency, under strongly stratified conditions. However, internal waves in near-homogeneous waters are restored by the Coriolis force, and f is no longer the lower frequency bound of the inertio-gravity wave band (LeBlond and Mysak 1978; Gerkema et al. 2008 for an overview). Second, as these near-inertial motions are the only internal waves that can pass from near-homogeneous to well-stratified layers, they can cause vertical turbulent exchange between these layers similar to slantwise-tilted convection tubes (Straneo et al. 2002; Sheremet 2004). They thus make the deep Mediterranean a rather actively varying region of water-mass properties (Testor and Gascard 2006; van Haren and Millot 2009). Third, the severe winters of 2005 and 2006 caused relatively deep dense-water formation in the northern Provençal and Ligurian subbasins of the Western Mediterranean (e.g., Schroeder et al. 2008; 2009). This resulted in newly formed water filling the basin from below, thereby pushing the less dense older near-homogeneous layer upwards and creating density stratification layers in the deep (van Haren and Millot 2009, see also some of their data reproduced in Fig. 1a here; Schroeder et al. 2009). Thus potentially, an internal wave band could be expected up to a large-scale (specified below) buoyancy frequency $N \approx 7f$ (around 2,200 m $N \approx 4f$), while stratification computed across smaller-scale "thin" layers has been observed occasionally as large as $N = 15$–$20f$ (inferred from data in Schroeder et al. 2009; data from van Haren and Millot 2009 reprocessed for Fig. 1b here).

In this paper, we present a yearlong time series of moored Acoustic Doppler Current Profiler (ADCP) observations between about 2,200 and 2,250 m, focusing on the direct observations of vertical currents for studying internal waves. The observations will demonstrate a variable internal wave band, which is different from that observed near the surface. They were made at the ANTARES neutrino telescope site in the Ligurian subbasin, 40 km south of Toulon, France (Ageron et al. 2011).

In a previous study (van Haren et al. 2011), combined optical (photomultiplier tube) and acoustic (ADCP) data from ANTARES were used to study the effects of vertical motions related to meso- and large-scale processes of mainly seasonal and 20 ± 10 day 'typical time-scale of occurrence' during 2006. These processes and time-scales were related to the meandering Northern Current, which flows counterclockwise along the boundary slopes of the Ligurian and Provençal subbasins and which is driven by buoyancy forces affected by rotation (Crépon et al. 1982, 1989; Albérola et al. 1995; Millot 1999). It is present throughout the year, but the strongest in the winter season when the density contrast is the largest between the near-coastal and basin-interior waters. This is because the latter is affected by dense-water formation.

Here, we will focus on higher-frequency motions having periodicities between 1 day, 17.6 h (local inertial period) and down to 20 min (maximum small-scale buoyancy period). Some consequences for turbulent mixing will be discussed.

2 Materials and methods

In 2007, the ANTARES Collaboration deployed and operated a so-called instrumentation line (Ageron et al. 2011) at the site 42° 48′ N, 06° 10′ E, 2,475-m water depth (Fig. 2). The ANTARES detector is one of a few deep-sea cabled networks. An electro-optical cable provides power and the connection for data transmission to and from a shore station (Aguilar et al. 2007). Such networks provide moored observations that are much less memory- and power-supply limited as in standard oceanographic stand-alone instrumentation. Cabled network observations can be made over very long periods of time, 10 years in the case of ANTARES.

The instrument line includes a downward-looking 300 kHz Teledyne-RDI ADCP at 2,190 m from which we analyze data covering the first full calendar year of operation (2008) here. The analysis focuses on internal waves as observed in vertical current (w) spectra ("Appendix"). The ADCP sampled data ensembles of 100 acoustic pings in 50 vertical bins of 2.5 m width roughly once per 10 min initially. In the winter of 2008, the sampling rate was increased to once per one minute, nominally. Data-transmission-to-shore interruptions (Fig. 3a) caused the effective sampling rates to be occasionally somewhat slower than set. For the present analysis we selected periods with thus few interrupts that affected the w-spectra well less than the confidence limits.

As the ADCP operates four beams, it offers an extra "error" velocity (e) that is composed of the difference between two w values estimated from the independent beam pairs (RDI 1992). Due to this definition, an error estimate is obtained for w in all coordinate frames using the distribution of e. These error estimates include horizontal-current inhomogeneities over the beam spread. An elaborate error analysis of w-data by the ADCP in this configuration is given by van Haren et al. (2011). This error analysis also includes tilt of the

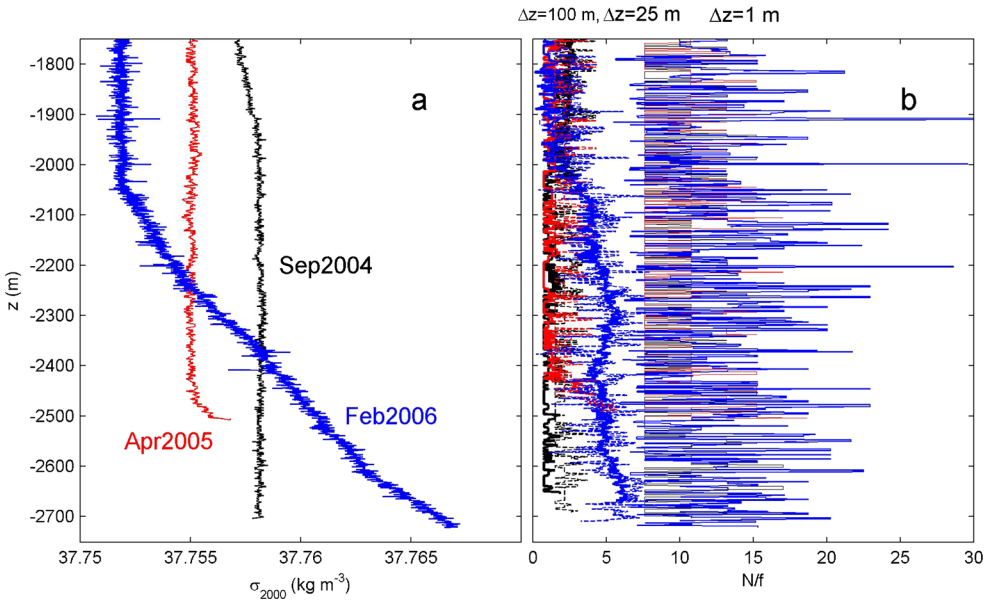

Fig. 1 CTD-parameter profiles as a function of depth from central West Mediterranean (40° N, 6° E), measured during three campaigns "Gyroscop" outside ANTARES. **a** Density anomaly (−1,000 kg m^{-3}), referenced to 2,000 m. **b** Buoyancy frequency in units of inertial frequency computed over Δz=1 m intervals (*thin lines*), over Δz=25 m (*dashed lines*), and over Δz=100 m (*thick lines*), positive definite values only. The blockades at about $N=7.5f$ in the Δz=1 m data and $N=1.3f$ in the Δz=25 m data are due to resolution of the instrumentation. Here, these values are equivalent to the accuracies in N for given vertical scale (van Haren and Millot 2006). The April 2005 profile stopped at 2,500 m because of cable shortage

instrumentation line, which was small over a yearlong period (<3°). It is not different for this data set.

3 Results

3.1 Yearlong time series

A yearlong time series of current data clearly shows a large difference between the horizontal and vertical current components (Fig. 3). The horizontal-current components (Fig. 3b, c) are dominated by variations that have an approximate 20-day timescale, which is associated with the Northern Current as in 2005/2006 observations (van Haren et al. 2011). The vertical currents (Fig. 3d) vary predominantly at shorter timescales of (much) less than a day, as will be shown in more detail below. The medium-scale vertical current shear, $S=(\Delta u/\Delta z, \Delta v/\Delta z)$ computed over a vertical range of Δz= 25 m, is typically weak ($|\boldsymbol{S}|=3\text{–}4\times10^{-4}$ $s^{-1}\approx 2\text{–}3f$) but can attain values exceeding 10×10^{-4} $s^{-1}\approx 7f$ (Fig. 3e).

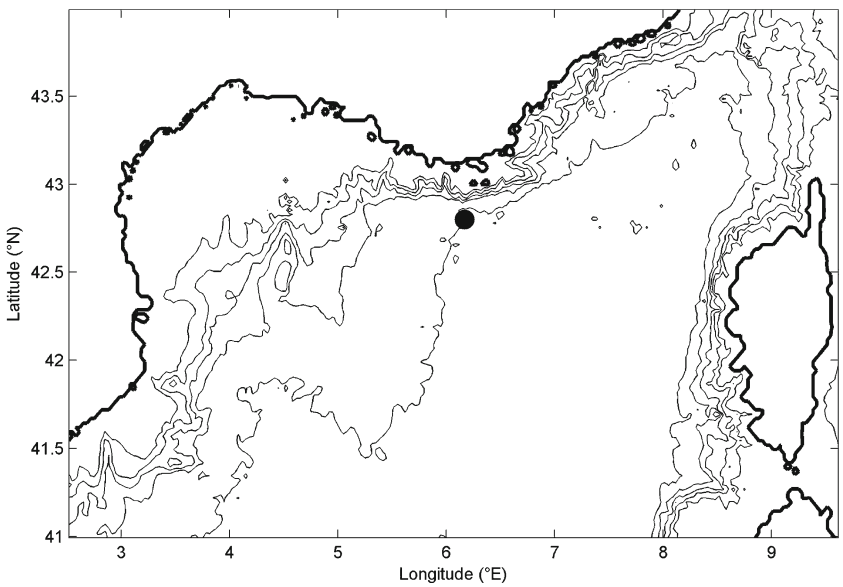

Fig. 2 ANTARES site (*dot*), which is located in the North-Western Mediterranean Sea off Toulon, France. *Isobaths* are drawn every 500 m between [−500, −2,500]m

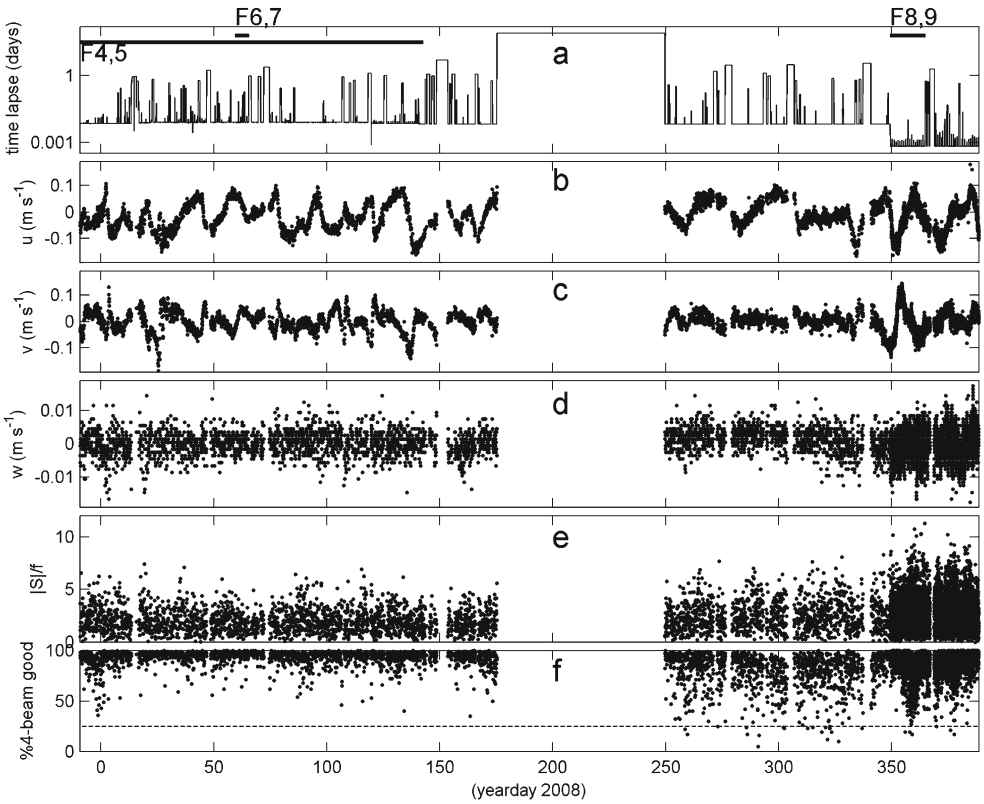

Fig. 3 Yearlong ANTARES–ADCP times series observed at 2,200 m (except for shear in **e**) in 2008, plotted every 10th data point. The *horizontal bars* with Fig. numbers indicate periods shown in more detail in Figs. 4–9. **a** Time lapse between observations, demonstrating the varying sampling rates and a large data gap in summer. **b** East–West current component. **c** North–South current component. **d** Vertical current component, after removal of overall mean. Note the different vertical scale compared to **b**, **c. e** Shear magnitude computed over 25 m, between 2,195 and 2,220 m, in units of local inertial frequency. **f** Percentage of all four beams providing good data. Lower values are associated with a decrease in reflecting particles. A standard threshold of 25 % is given by the *dashed line*

The relatively short range used for computing the shear is related to the occasionally low numbers of acoustic scatterers, which limits the amount of good data especially in the second half of the year (Fig. 3f). This percentage of good (all-four-beams) data not only varies with time, but it varies also with distance from the ADCP, and when it hits a hard target like another instrument in the line (Fig. 4a). Below, only data will be considered when the all-four-beams percentage of good data exceeds the standard threshold, which is generally found for $z>-2{,}250$ m. The shear magnitude $|\boldsymbol{S}|(t)$ (Fig. 3e) is of the same order as estimates of $N(z)$ computed over $\Delta z=25$ m using CTD data (Fig. 1b, thick lines).

3.2 Winter/spring detail

The relatively weak mean shear may also be directly inferred from the rather small vertical phase changes between variations in depth-time series of the first 150 days (Fig. 4). These series show the same discrepancy between horizontal and vertical currents as noted from Fig. 3, with dominant low-frequency variations in the former (Fig. 4b) and dominant high-frequency variations in the latter (Fig. 4c). In the mean spectra (Fig. 5) of this period when average sampling was 780 s, this discrepancy is clearly visible. The KE-spectrum (blue) steadily decreases from its, in this period here, 17-day periodicity peak, at a rate of about σ^{-2} for $0.05<\sigma<7$ cpd (cycles per day, 1 cpd$=2\pi/86{,}400$ s^{-1}) with the exception of a near-inertial peak. For $\sigma<f$, the w-spectrum (red) is almost flat, and for $\sigma>f$, the steady drop is at an approximate rate of σ^{-1}. Thus, high-frequency motions ($\sigma\sim N_{100}$, see "Appendix" for definition of this large-scale buoyancy frequency) are more energetic relatively to low-frequency motions in the vertical than in the horizontal currents. Their variance ratio averages about 0.5 near N (Fig. 5b), as expected.

Using the flat, white noise spectrum of the error velocity (green) for reference, the w-spectrum is observed to exceed e's constant variance level for $\sigma<28$ cpd$=N_{\mathrm{mADCP}}$ (Fig. 5a; see "Appendix" for this maximum small-scale buoyancy frequency). Obviously, this frequency cutoff depends on the level of instrument noise and on the internal wave variance (exceeding the white noise level). Here, N_{m} follows from ADCP's w-spectrum, not from CTD data. The significant extent of the w-spectrum above the e-spectrum and the difference between slopes in w- and KE-spectra demonstrate that vertical currents are well measured by the ADCP and not artificially dependent on horizontal currents, for most of the internal wave range. The nearly constant slope of σ^{-1} for $\sim 1.1f<\sigma<22$ cpd is interrupted around $\sigma\approx 4.4$ cpd$=N_{100\mathrm{ADCP}}$. This definition of N_{100} (labelled as "N" in Fig. 5; *cf* "Appendix") is commensurate with the general notion that the w-spectrum rolls off for $\sigma>N$ (Cairns and Williams 1976; Pinkel 1981), except that the spectral peak commonly found at $0.5N$ in open-ocean and near-surface data is not observed here. As for N_{m} above,

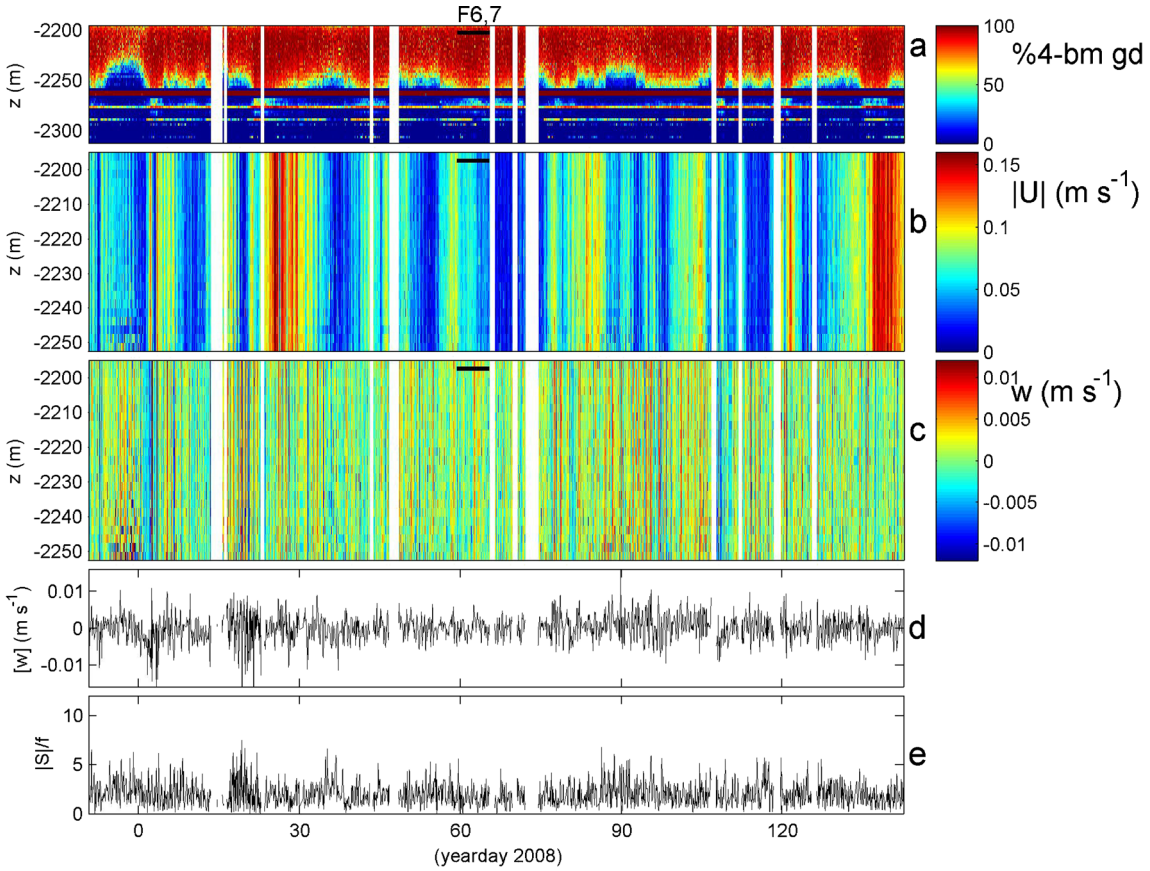

Fig. 4 First 5 months of ANTARES–ADCP depth-time series observed in 2008, plotted every 10th data point. *White gaps* indicate time lapses >0.5 day. **a** Percentage of good data when all four beams are working properly, over full range of observations. The range of good data >25 % is approximately between 2,192.5 and 2,252.5 m, except during brief periods like around the beginning of the year (day 0) when it rises to about 2,230 m. *Horizontal lines* indicate bad data due to acoustic obstructions of other instruments in the line. **b** Horizontal current magnitude for 60 m range of generally good data, note the different vertical scale compared to the *upper panel*. **c** Vertical current component over 60 m range. **d** Vertical average of **c** over the 25 m range of permanently good data, between 2,195 and 2,220 m. **e** Shear magnitude as in Fig. 3e

N_{100} follows from ADCP's *w*-spectrum here, not from CTD data.

The rather-broad near-inertial peak extends to subinertial frequencies in such a way that the subinertial slope approaches σ^{+1} for 0.5 cpd$<\sigma<\sim 1.1f$. The lower bound (0.5 cpd) of this frequency band is approximately equivalent to the lower bound of the inertio-gravity wave band for very weak stratification $N_{100\mathrm{CTD}}=0.5f$ (see LeBlond and Mysak 1978; Gerkema et al. 2008 for the definition of the "non-traditional" inertio-gravity wave limits). This weak stratification value is observed using CTD data in near-homogeneous layers in the deep Mediterranean (van Haren and Millot 2006; van Haren and Gostiaux 2011). This explains the extension of the inertio-gravity internal wave band to this frequency, at which apparently waves do not often occur. The more-often-occurring internal wave frequencies fill the *w*-spectral peak. This broad near-inertial *w*-peak fits more or less between the dashed light-blue inertio-gravity wave frequency bounds for a mean $N_{100\mathrm{CTD}}=f$ (Fig. 5), which thus indicates the typical stratification. The extent of the *w*-spectrum into even lower frequencies $\sigma<0.5$ cpd having variance above the σ^{+1}-slope may be partially related to inertio-gravity wave motions under purely homogeneous conditions. Such motions have a maximum range $0<\sigma<2\Omega$, Ω the Earth rotational frequency. However, this part of the *w*-spectrum is more likely related to mesoscale meanders or eddies (we cannot distinguish between the two from single mooring data) of roughly 20±10 day 'typical time-scale of occurrence' that are associated with newly formed dense deep water enforcing the boundary current (Crépon et al. 1982; 1989), as discussed in van Haren et al. (2011). These "eddy"-periodicities, in the example here peaking at 0.06 cpd, are best visible in (horizontal) kinetic energy (blue in Fig. 5). Their rather broad (insignificant peak) frequency-range-distribution for vertical currents, compared with the horizontal current peak, suggests that vertical and horizontal currents are differently distributed in meanders and eddies. Previous observations suggest that *w*-peak along the rim of eddies, whereas horizontal currents are found enhanced over a larger spatial area (van Haren et al. 2006; van Haren et al. 2011).

The KE-spectrum (blue) shows more variance at subinertial $\sigma<f$ than both the *w*-spectrum (Fig. 5b; as discussed) and the shear spectrum (black). The latter

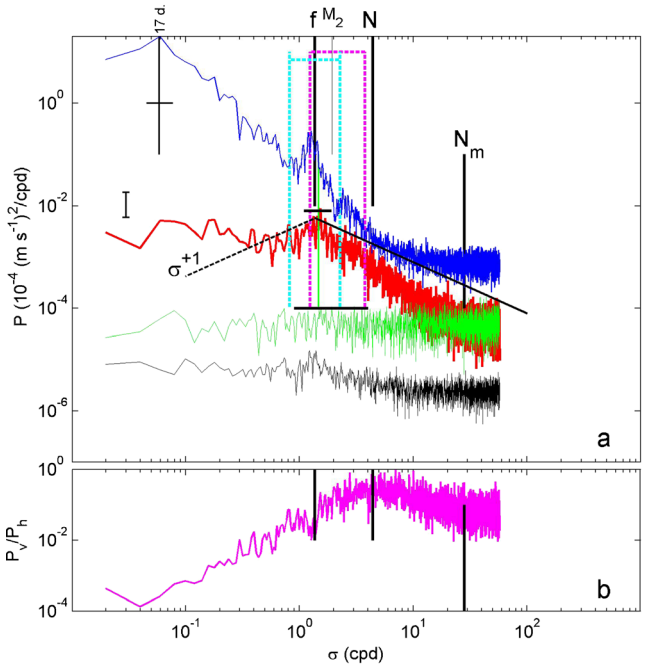

Fig. 5 Power spectra of ADCP data for the period in Fig. 4 in cycles per day. **a** In *red*, the vertical current spectrum at 2,210 m is given; in *green*, the corresponding error velocity. In *blue*, the corresponding kinetic energy is given, and in *black*, the 25-m shear spectrum (units 10^{-4} s^{-2}/cpd). The *horizontal black lines* indicate levels of maximum $\Phi_w(f)$ and noise (*top* error velocity, *green* spectrum). Several frequencies are indicated in the internal wave band by *vertical black lines*. The *vertical green line* indicates f_h, the local frequency for horizontal Coriolis parameter. Two special frequencies are the following: the frequency where the spectrum Φ_w deviates from the σ^{-1}-slope is labelled "*N*", the frequency where Φ_w reaches noise level is labelled "N_m". For reference, one semidiurnal tidal frequency (M_2) is given, two spectral slopes and two inertio-gravity wave bands, for $N=1f$ (*light-blue lines*) and for $N=2.5f$ (*purple*). The *vertical black bar* indicates the 95 % confidence limits. **b** Ratio of vertical (*red spectrum* in **a**) over horizontal (*blue spectrum* in **a**) current variance

resembles more the *w*-spectrum. Subtle differences are observed in the near-inertial peak frequency, being just subinertial for the kinetic energy ($0.9f$, or the lower bound of the inertia-gravity band for $N_{100}\approx 2.5f$) and approximately $0.95f$ for the shear spectrum. In contrast, the *w*-spectrum peaks (non-significantly) at about $1.1f$, close to the horizontal Coriolis parameter f_h (green line). These peak-frequency differences can be understood in terms of quasi-gyroscopic inertio-gravity waves in near-homogeneous waters.

3.3 Six-day detail of low variance

In further detail during a relatively quiescent, low-shear period of six days in spring, inertial-period motions are seen in both horizontal (Fig. 6b) and vertical currents (Fig. 6c, d). In these 10-min-sampled ensemble data, the period of dominant near-inertial motions is not very fixed, so that the poorly resolved spectra (Fig. 7) do not show well-discernible inertial peaks but rather broad bands. Compared to the 150-day average spectra of Fig. 5, this 6-day period shows about half a decade lower near-inertial "peak" in the *w*-spectrum, along with reductions in KE(f)- and $\boldsymbol{S}(f)$-spectral peaks and in both $N_{100ADCP}$ and N_{mADCP}. The thus-determined $N_{100ADCP}\approx 2.3f$, nearing f, but $N_{mADCP}\approx 11f$, still one decade from f. The latter suggests occasionally occurring high-frequency coherent motions of about 2-h period ($\sigma\approx 8f$), which we localize having large amplitude around day 60.15 in Fig. 6c, d (especially in the latter). This is not associated with a local increase in shear, but rather a local minimum (Fig. 6e). In the vertically averaged record, further 2-h-period motions of small amplitude are observed between days 61 and 62 mainly (Fig. 6d). Groups of about 2 waves of about 9-h period ($\sigma\approx 2f$) are observed around days 62 and 65. In contrast with the 150-day period, the ratio of vertical over horizontal current variance is largest around N_m, where an average of about 0.7 is observed (Fig. 7b).

3.4 Two-week detail of high variance, sampled at a rate of 1 min

A nearly continuously high-sampled (~60 s) period of a fortnight in winter shows similar features, but with less reflecting particles (Fig. 8a) and higher amplitudes in all current components (Fig. 8b–d) and shear (Fig. 8e). Besides showing more variance, the noise-exceeding part of the *w*-spectrum is shifted to higher frequencies: $N_{100ADCP}=6.2$ cpd$\approx 4.5f$, $N_{mADCP}=78$ cpd (Fig. 9). As in the half-yearlong mean spectrum of Fig. 5, this two-week-period *w*-spectrum has approximate slopes σ^{+1} for 0.5 cpd$<\sigma<1.2f$ (peak); σ^{-1} for $1.2f<\sigma<6$ cpd and 12 cpd$<\sigma<78$ cpd, with a break in between; and σ^{-3} for 6 cpd$<\sigma<12$ cpd. Also, the ratio of vertical over horizontal current variance peaks around large-scale N, not small-scale N_m as in the previous subsection. Around N, it now averages about 0.9. Note the roll-off into a white noise spectrum around the theoretical value (dashed horizontal line) related with the ADCP's slanted beam angle of 20° for $\sigma>N_m$.

As for coherent small-scale *w*-motions (say, high-frequency internal waves), a small group is visible in Fig. 8d around day 364.3: it has about a 1-h periodicity and $|w|=5\times10^{-3}$ m s^{-1} amplitudes. Evidence of significantly observed high-frequency coherent internal wave motions is provided in Fig. 10, in which $|w|=2\times10^{-3}$ m s^{-1} amplitude motions have periods down to 1,110 s commensurate $N_{mADCP}=78=86{,}400/1{,}110$ cpd. These high-frequency motions have a vertical extent which is less than the range of 60 m in Fig. 8c, but still reach typically 20 m. They occur in groups of 3–4 waves, typically intermittent for internal waves. No clear relationship with low-frequency shear is observed, of which the magnitude varies between about 2 and $4f$ for the three cases (cf. Fig. 8e).

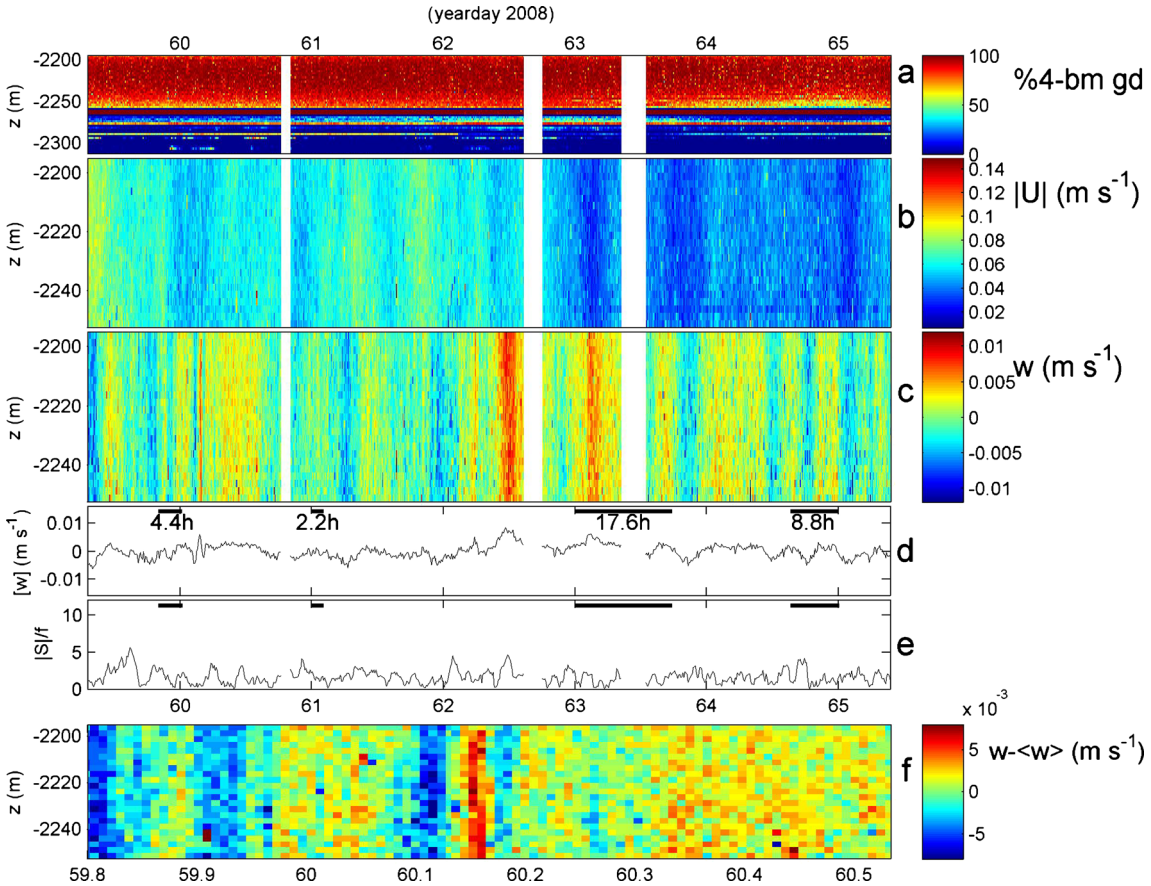

Fig. 6 As Fig. 4, but for 6 days when time-mean 25-m shear was low, $<|\boldsymbol{S}|>=1.7f$. Here, *white gaps* indicate time lapses >1.5 h. The local inertial period ($T_f=2\pi/f\approx17.6$ h) is indicated, as well as $0.5T_f$, $0.25T_f$, $0.125T_f$ (corresponding to frequencies $2f$, $4f$, $8f$, respectively). In **f**, a 1.0Tf-zoom is given of **c** around the large 2-h period internal wave, with respect to the time mean (color-scale slightly changed with respect to the one of **c**)

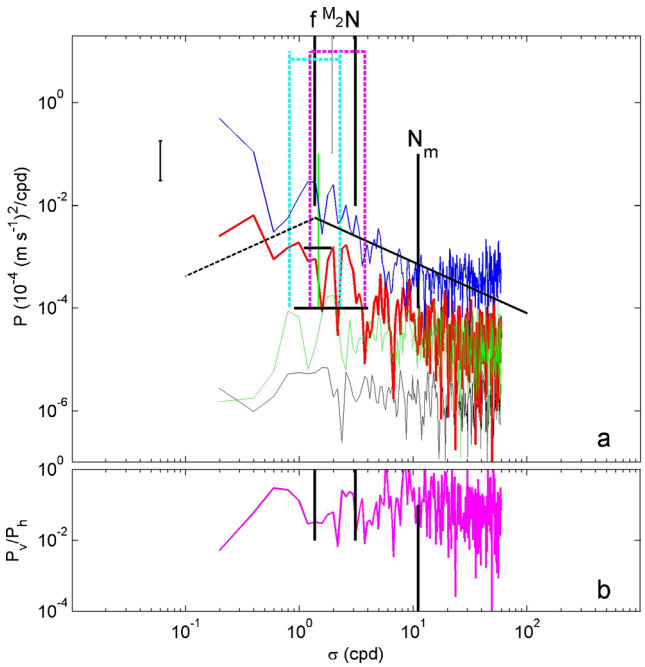

Fig. 7 As Fig. 5 with the same reference slopes and inertio-gravity wave bands, but for different N, N_m for the period of Fig. 6

4 Discussion

The present observations demonstrate the existence of high-frequency internal waves in the deep Mediterranean Sea. The observed internal wave frequency range of the direct vertical current observations using the moored ANTARES–ADCP matches well with the "Gyroscop" CTD-observed range of buoyancy frequencies representing stratification. As the CTD observations were made during different periods, they demonstrate a common universality in deep Mediterranean high-frequency internal waves. The range of buoyancy frequencies also matches the variation with time of ADCP-observed large-scale vertical current shear. The low-frequency, subinertial shear, and stratification variations have an impact on the internal wave propagation, with a well-observed N scaling of the vertical current spectrum and an unusual σ^{-1} slope for $N<\sigma<N_m$ as a result. It is noted that the present single mooring observations do not, and are not expected to, provide a direct correlation between these high- (super-large-scale-buoyancy-) frequency internal waves and low-frequency shear. This is because the low-frequency shear is coupled with large-scale N, not necessarily with small-scale N_m. Small-scale waves

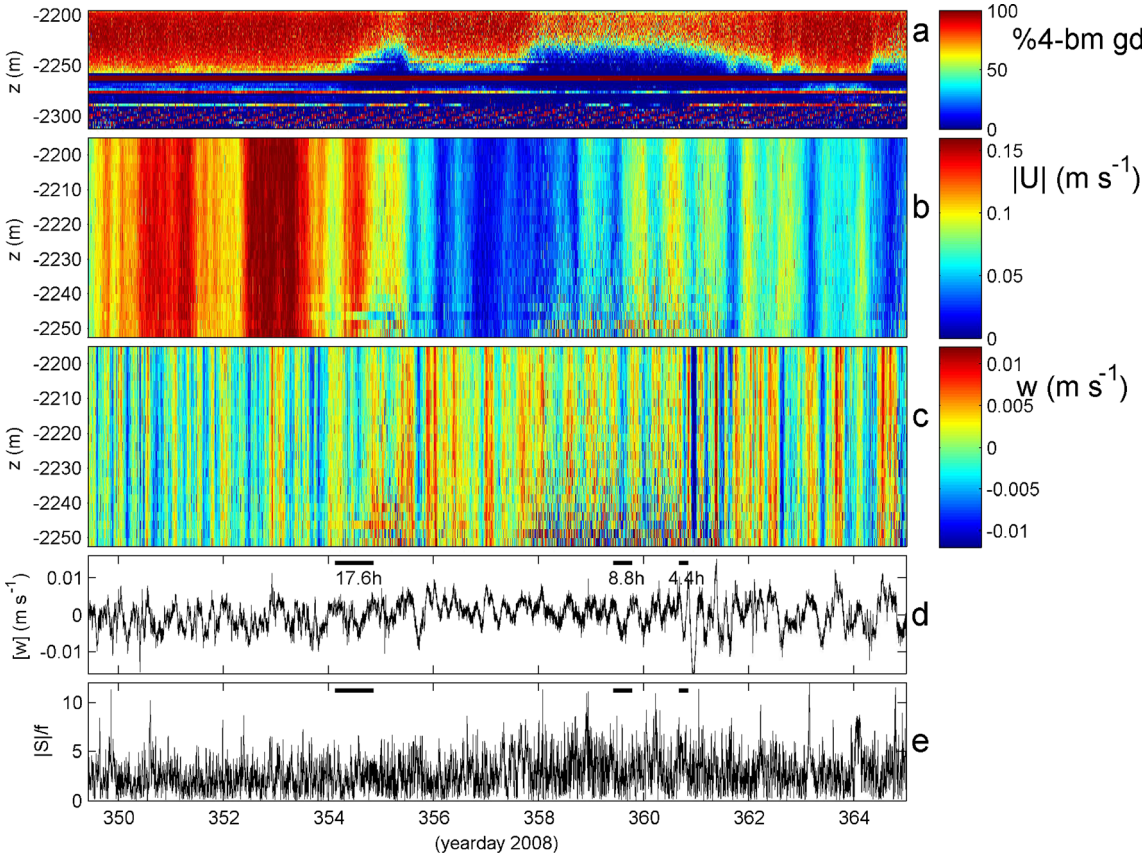

Fig. 8 As Fig. 4, but for 15 days near the end of the year, when sampling rate was highest (~60 s), artificial time lapses small and far between, and 25-m mean shear relatively high $<|\boldsymbol{S}|>=2.9f$ with incidental values up to $|\boldsymbol{S}|\approx 10f$

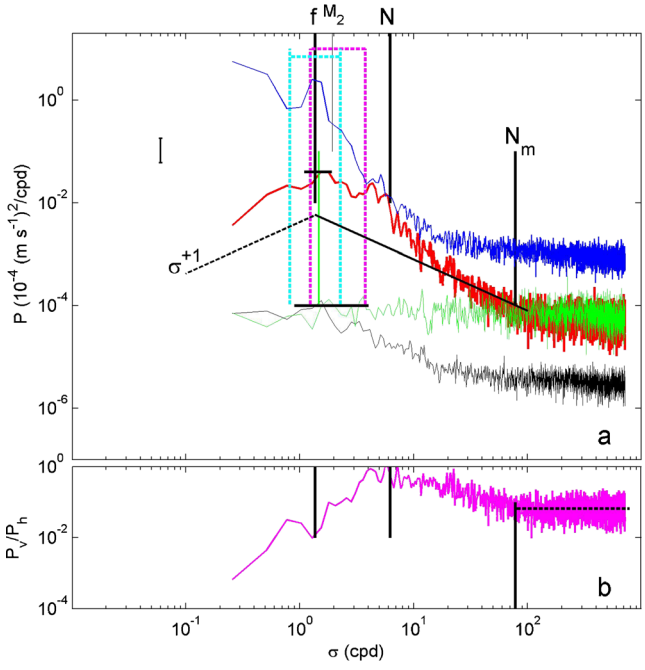

Fig. 9 As Fig. 5 with the same reference slopes and inertio-gravity wave bands, but for different N, N_m for the period of Fig. 8. **b** The *horizontal dashed line* indicates the theoretical (manufacturer's) noise level variance ratio

may become destroyed via Kelvin–Helmholtz shear-induced turbulence; loss of large-scale shear may enhance high-frequency internal waves. Furthermore, the precise sources and propagation paths of the internal waves cannot be established from the one-dimensional short-range observations. Future research should be based on three-dimensional (mooring array) observations.

The w-spectral peak near (1.1–1.2)f is at unusually low frequency compared to open upper ocean w-humps near the buoyancy frequency $N>10f$ (Cairns and Williams 1976; Munk 1980; Pinkel 1981). Apparently, the near-homogeneous layers above and below thin strongly stratified layers continue to dominate internal wave motions resulting in a w-spectral peak at about $0.5N$, $N=N_{100}\approx 2.2f$, despite the locally enhanced stratification in the thin layers. The extension of significant coherent w-motions to higher frequencies (observed up to 78 cpd) is associated with growth in variance and, presumably but not necessarily, increasing shear and stratification. In fact, taking previous spectra in near-homogeneous waters into account (van Haren and Millot 2005), one finds a positive power law in N for the w-spectrum $\Phi_w(\sigma) \propto N^4\sigma^{-1} \propto N_m{}^{1.5}\sigma^{-1}$ for near-f-peak$<\sigma<$N ($<N_m$). This is counterintuitive from the general ocean perspective of density stratification as the restoring force in an equilibrium internal wave field. The above power law is quite different from the negative

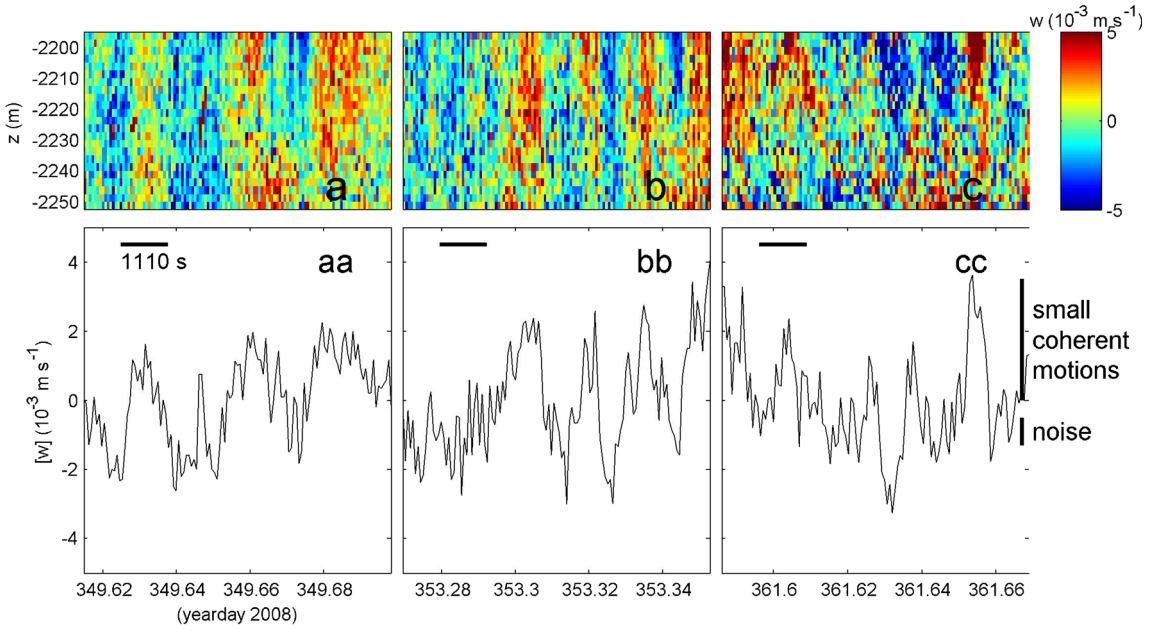

Fig. 10 Three 2-h periods of vertical currents, with respect to their local time mean, from Fig. 8c (**a**–**c**) and Fig. 8d (**aa**–**cc**: here, vertical average is over full range of 60 m in **a**–**c**); the shortest period T_{Nm}=1,110 s. *Bars* to the *right* indicate approximate amplitude scales of vertically coherent motions and of noise

power law in N for open ocean, near-surface spectra in the range $f<<\sigma<<N$ (Munk 1980), but rather close to shallow sea, quasi two-layer spectral observations (van Haren 2008). From the present data, it is estimated that the transition between the two regimes is found for (at least) $N\sim6$ cpd, the largest large-scale buoyancy frequency for the present observations.

The present KE-spectra compare to within a factor of 2 with those from other deep Western-Mediterranean observations (van Haren and Millot 2004). As was indicated by van Haren and Millot (2004), their KE-spectra between 100 and 2,700 m followed a reasonable N-scaling for levels where $N\geq 2.5f$, with the exception of data from levels where $N\sim0$. They verified (but did not publish) that the ($N\geq2.5f$)-spectra collapse to the canonical "GM" (Garrett and Munk 1972) internal wave variance to within a factor of 2, provided the GM-vertical-scale b was used from the range of weakest stratification instead of from around 1,000 m. For levels where $N\sim0$, the GM-model principally would not work, but van Haren and Millot (2004) suggested a collapse to within a factor of 2 after using an artificial scaling factor of $N=3f$.

Our observations thus confirm that the deep Mediterranean is a more active internal wave and internal wave-induced turbulent sea rather than being quiescent, as has been recently demonstrated for the central Western Mediterranean mainly using CTD observations (van Haren and Millot 2009) and for the Eastern Mediterranean using high-resolution temperature sensors (van Haren and Gostiaux 2011). In all cases, mixing seems to be governed by inertial wave motions as expected, because they are the only waves that can freely propagate in both stratified and near-homogeneous waters. They are associated with previously observed mesoscale eddy variability which can be vigorous in the deep Mediterranean when enforced by dense-water formation (Gascard 1973; Taupier-Letage and Millot 1986; Testor and Gascard 2006). The varying dynamics in the Mediterranean suggest that the above observations are expected to exist in various other sites outside the Ligurian Sea.

Acknowledgments The CTD observations were made in the framework of "Gyroscop" and "Gyroscop-2" for which we acknowledge Claude Millot and the Netherlands Organisation for the Advancement of Scientific Research, NWO, and Centre National de la Recherche Scientifique, CNRS, for support (French–Dutch collaboration). The authors acknowledge the financial support of the funding agencies: Centre National de la Recherche Scientifique (CNRS), Commissariat à l'énergie atomique et aux énergies alternatives (CEA), Commission Européenne (FEDER fund and Marie Curie Program), Région Alsace (contrat CPER), Région Provence-Alpes-Côte d'Azur, Département du Var and Ville de La Seyne-sur-Mer, France; Bundesministerium für Bildung und Forschung (BMBF), Germany; Istituto Nazionale di Fisica Nucleare (INFN), Italy; Stichting voor Fundamenteel Onderzoek der Materie (FOM) and NWO, the Netherlands; Council of the President of the Russian Federation for young scientists and leading scientific schools supporting grants, Russia; National Authority for Scientific Research (ANCS -UEFISCDI), Romania; Ministerio de Ciencia e Innovación (MICINN), Prometeo of Generalitat Valenciana and MultiDark, Spain; Agence de l'Oriental and CNRST, Morocco. We also acknowledge the technical support of Ifremer, AIM, and Foselev Marine for the sea operation and the CC-IN2P3 for the computing facilities.

Appendix

Short review of internal wave signatures in shipborne CTD data and moored vertical current observations

Shipborne conductivity-temperature-depth CTD-profile observations are a practical means to establish the possible existence of internal waves without observing their propagation directly. CTD data are used to compute the density stratification of natural stability, which provides the upper limit of the internal wave frequency band. The buoyancy frequency $N=N_{100}$, computed over a typical but arbitrary large (vertical) scale of $\Delta z=100$ m using a first-order difference scheme, is a measure for the overall, smoothed "background" stratification. In more detail, single profile stratification is in thin strongly stratified layers with larger, more-homogeneous layers in-between. Such layering is created by, e.g., turbulent mixing and straining of the larger-scale (low-frequency) internal waves. Thus, when the vertical density stratification is computed over smaller vertical scales, say $\Delta z=1$ m, a wider variety of buoyancy frequencies, although at larger accuracy, is observed from a minimum smaller than N_{100} and up to a maximum $N_1=N_m$ (Fig. 1b). Thereby, the error of computation increases of course, which is verified to be about $0.8f$ for 100 m range (van Haren and Millot 2006) and thus about $8f$ for 1 m range.

The small-scale buoyancy frequencies $>N_{100}$ could support small-scale internal waves that propagate along thin interfaces. The large-scale N are thought to support internal wave groups with frequencies $\sigma<N_{100}$ in a more three-dimensional fashion. These wave groups can reflect at layers where $N_{100}(z)$ becomes smaller than their frequencies (Munk 1980). The enhanced energy due to reflection is thought to create a hump in potential energy (or vertical current) spectra, as modelled using Airy functions by Munk (1980) and which is commonly found to peak at $\sigma=0.5N$ (Cairns and Williams 1976). In the upper 200 m of the Mediterranean $N_{100}=10$–$100f$ and the internal wave frequency band is one to two decades wide.

Low-frequency internal waves near f are best studied by exploring kinetic energy spectra, Φ_{KE}, from moored horizontal-current observations. High-frequency internal waves near N are best studied by exploring potential energy spectra $\Phi_{PE}=N^2\Phi_\eta$ from density-layer displacement spectra Φ_η, e.g., inferred from temperature observations (Munk 1980). Alternatively for the latter, one can use vertical current observations, given the relationship $w=d\eta/dt$ (e.g., Fofonoff 1969), so that w-spectra $\Phi_w=(\sigma^2/N^2)\Phi_{PE}$. Classically, for open-ocean near-surface internal waves in the frequency range $f<<\sigma<<N$, the spectrum $\Phi_w(\sigma, z) \sim N(z)^{-1}$ is a constant with frequency and decreases its variance when (large-scale) N increases (Munk 1980). This relationship obviously fails in homogeneous waters. Direct vertical current observations are rather rare, because in general the oceanic aspect ratio of vertical over horizontal currents is low, being O(0.001–0.01). It is noted that this aspect ratio becomes larger for internal waves, being O(0.01–0.1) for low-frequency internal waves in moderate-strong stratification. It approaches 1 for internal waves near the buoyancy frequency in general and for near-inertial waves in near-homogeneous waters (van Haren and Millot 2005), just like in turbulent motions.

References

Ageron M, ANTARES collaboration et al (2011) ANTARES: the first neutrino telescope in the Mediterranean Sea. Nucl Inst Methods Phys Res A 656:11–38

Aguilar JA, ANTARES collaboration et al (2007) The data acquisition for the ANTARES neutrino telescope. Nucl Inst Meth Phys Res A 570: 107–116

Albérola C, Millot C, Font J (1995) On the seasonal and mesoscale variabilities of the Northern Current during the PRIMO-0 experiment in the western Mediterranean Sea. Oceanol Acta 18:163–192

Cairns JL, Williams GO (1976) Internal wave observations from a midwater float, 2. J Geophys Res 81:1943–1950

Crépon M, Wald L, Monget JM (1982) Low-frequency waves in the Ligurian Sea during December 1977. J Geophys Res 87:595–600

Crépon M, Boukhtir M, Barnier B, Aikman F III (1989) Horizontal ocean circulation forced by deep-water formation. Part I: an analytical study. J Phys Oceanogr 19:1781–1792

Fofonoff NP (1969) Spectral characteristics of internal waves in the ocean. Deep-Sea Res 16:58–71

Garrett CJR, Munk WH (1972) Space-time scales of internal waves. Geophys Fluid Dyn 3:225–264

Gascard J-C (1973) Vertical motions in a region of deep water formation. Deep-Sea Res 20:1011–1027

Gerkema T, Zimmerman JTF, Maas LRM, van Haren H (2008) Geophysical and astrophysical fluid dynamics beyond the traditional approximation. Rev Geophys 46:RG2004. doi:10.1029/2006RG000220

LeBlond PH, Mysak LA (1978) Waves in the ocean. Elsevier, Amsterdam

Millot C (1999) Circulation in the Western Mediterranean Sea. J Mar Syst 20:423–442

Munk WH (1980) Internal wave spectra at the buoyant and inertial frequencies. J Phys Oceanogr 10:1718–1728

Pinkel R (1981) Observations of the near-surface internal wavefield. J Phys Oceanogr 11:1248–1257

RDI (1992) A practical primer. RD-Instruments, San Diego

Schroeder K, Ribotti A, Borghini M, Sorgente R, Perilli A, Gasparini GP (2008) An extensive Western Mediterranean deep water renewal between 2004 and 2006. Geophys Res Lett 35:L18605. doi:10.1029/2008GL035146

Schroeder K, Gasparini GP, Borghini M, Ribotti A (2009) Experimental evidence of recent abrupt changes in the deep Western Mediterranean Sea. CIESM Workshop Monographs, n°38: Dynamics of Mediterranean deep waters, Malta, 27–30 May 2009:51–56

Sheremet VA (2004) Laboratory experiments with tilted convective plumes on a centrifuge: a finite angle between the buoyancy and the axis of rotation. J Fluid Mech 506:217–244

Straneo F, Kawase M, Riser SC (2002) Idealized models of slantwise convection in a baroclinic flow. J Phys Oceanogr 32:558–572

Taupier-Letage I, Millot C (1986) General hydrodynamic features in the Ligurian Sea inferred from the DYOME experiment. Oceanol Acta 9:119–132

Testor P, Gascard J-C (2006) Post-convection spreading phase in the Northwestern Mediterranean Sea. Deep-Sea Res I 53:869–893

van Haren H (2008) A comparison between vertical motions measured by ADCP and inferred from temperature data. Ocean Sci 4:215–222

van Haren H, Gostiaux L (2011) Large internal waves advection in very weakly stratified deep Mediterranean waters. Geophys Res Lett 38: L22603. doi:10.1029/2011GL049707

van Haren H, Millot C (2004) Rectilinear and circular inertial motions in the Western Mediterranean Sea. Deep-Sea Res I 51:1441–1455

van Haren H, Millot C (2005) Gyroscopic waves in the Mediterranean Sea. Geophys Res Lett 32:L24614. doi:10.1029/2005GL023915

van Haren H, Millot C (2006) Determination of buoyancy frequency in weakly stable waters. J Geophys Res 111:C03014. doi:10.1029/2005JC003065

van Haren H, Millot C (2009) Slantwise convection: a candidate for homogenization of deep newly formed dense waters. Geophys Res Lett 36:L12604. doi:10.1029/2009GL038736

van Haren H, Millot C, Taupier-Letage I (2006) Fast deep sinking in Mediterranean eddies. Geophys Res Lett 33:L04606. doi:10.1029/2005GL025367

van Haren H, ANTARES-collaboration et al (2011) Acoustic and optical variations during rapid downward motion episodes in the deep north-western Mediterranean Sea. Deep-Sea Res I 58:875–884